International Journal of Applied Earth Observations and Geoinformation 102 (2021) 102394

Contents lists available at ScienceDirect

International Journal of Applied Earth Observations and Geoinformation

journal homepage: www.elsevier.com/locate/jag

Satellite observed rapid green fodder expansion in northeastern Tibetan Plateau from 2010 to 2019

Tong Yang [a], Geli Zhang [a,*], Yuzhe Li [b], Jiangwen Fan [b], Danfeng Sun [a], Jie Wang [c], Yuanyuan Di [a], Nanshan You [b], Ruoqi Liu [a], Qiang Zhang [a], Russell B. Doughty [d]

[a] College of Land Science and Technology, China Agricultural University, Beijing 100193, China
[b] Key Laboratory of Land Surface Pattern and Simulation, Institute of Geographic Sciences and Natural Resources Research, Chinese Academy of Sciences, Beijing 100101, China
[c] College of Grassland Science and Technology, China Agricultural University, Beijing 100193, China
[d] Division of Geological and Planetary Sciences, California Institute of Technology, Pasadena, CA 91125, USA

ARTICLE INFO

Keywords:
Green fodder mapping
Pixel- and phenology-based approach
Google Earth Engine (GEE)
Landsat
Northeastern Tibetan Plateau
Rapid expansion

ABSTRACT

The livestock product consumption per capita in China has almost doubled in the past three decades. The planting of green fodder has increased in the agropastoral ecotone of China to meet the increasing demand for livestock feed, and the green fodder expansion can have subsequent consequences on the environment. However, information on the area and distribution of green fodder is very limited. Here, we developed a pixel- and phenology-based algorithm to map green fodder and track its dynamics in the northeastern Tibetan Plateau, a typical alpine pasture region in China, using all the available Landsat images and Google Earth Engine (GEE). We developed a simple approach for the rapid identification of green fodder fields by using a new green fodder index that considers the unique phenology of green fodder, which has higher greenness and water content in the late growing season than other vegetation. A total of 858 Landsat images were used to generate green fodder maps in northeastern Tibetan Plateau (including Zeku, Guinan, and Tongde Counties) in three periods (*circa* 2010, 2015, and 2019). The overall accuracies of our green fodder maps were 93–97% and the Matthews correlation coefficients were 0.76–0.83. We found a rapid expansion of green fodder from 16.3 km^2 in 2010 to 136.1 km^2 in 2019. Newly cultivated green fodder occurred in both existing croplands and natural grasslands. Our study demonstrated the potential of the phenology-based approach, all the available Landsat images, and GEE for tracing the historical dynamics of green fodder at 30-m resolution in alpine regions. Our findings advance our understanding of changes in forage area, production, the supply–demand gap, and the ecological and climatic consequences of green fodder expansion.

1. Introduction

Human food consumption has shifted towards more high-quality and luxurious goods instead of necessities over the past decades (Kearney, 2010; Sheng and Song, 2019; Tilman and Clark, 2014). In China, grain consumption per capita decreased from 237.9 kg/yr to 125.6 kg/yr (-47.2%) during 1984–2018, while livestock product consumption per capita increased from 26.7 kg/yr to 51.4 kg/yr (+92.7%) according to the official statistical data of China (http://www.stats.gov.cn/). The accelerated demand for livestock products imposes great pressure on forage supply and has deteriorated the grain competition between humans and animals (He et al., 2019; Sheng and Song, 2019; Zhai et al., 2019). Green fodder, fresh crops like alfalfa, silage corn, forage oat, and ryegrass with richer nutrients and more water content (Zhai et al., 2019), are critical for alleviating the forage shortage. Since 2016, the National Plan for Crop Production Structural Adjustment in 2016-2020 of the Ministry of Agriculture in China emphasized the development of forage production for animal husbandry and encouraged the planting of high-quality forage crops. Despite the importance of data on forage production, the existing data is limited to statistical data, and studies of the area and spatial distribution of fodder crops in China are scant.

The Tibetan Plateau (TP), described as the largest plateau in the world, is the headwaters of major rivers, and a climate indicator for East Asia (Che et al., 2014; Chen et al., 2014), and hosts various ecosystems

* Corresponding author at: College of Land Science and Technology, China Agricultural University, Beijing 100193, China..
E-mail address: geli.zhang@cau.edu.cn (G. Zhang).

https://doi.org/10.1016/j.jag.2021.102394
Received 4 March 2021; Received in revised form 4 June 2021; Accepted 8 June 2021
Available online 17 June 2021

that are sensitive to climate change and human activities. Alpine grasslands dominated land cover vegetation over the TP (Chen et al., 2014). However, the grassland degradation in TP has been widely documented for a very long time (Liu et al., 2008) and overgrazing is mostly considered as the major cause of the degradation (Harris, 2010; Li et al., 2013), posing even more pressure on its harsh and vulnerable ecosystem (Zhang et al., 2017). A shortage of 37% energy required by livestock was reported in the TP during the winter, which can lead to livestock malnourishment and mortality (Abdelraheem et al., 2019; Xue et al., 2005). The increasing demands for forage have become a regional dilemma faced by the livestock industry. Green fodder, mainly oat and rapeseed, has been cultivated to meet the increasing demands for animal forage in northeastern TP (Li et al., 2020), which is a typical alpine agricultural-pastoral region with highly eco-fragile conditions (Tang et al., 2018). Despite comprising a small share of crops in the region, green fodder expansion has led to ecological consequences, which have been largely ignored (Chen et al., 2010; Waldner et al., 2019). Here we developed a novel approach to map green fodder and track its spatio-temporal expansion, expecting to improve our understanding of the regional imbalance between forage supply and demand, and to support regional agriculture and pasture management.

Traditional small-scale field surveys using quadrats and statistical analysis methods are inadequate for monitoring the spatio-temporal pattern and long-term green fodder dynamics at the regional scale (Zhai et al., 2019). Satellite remote sensing has become an invaluable tool for tracking land cover and land use dynamics. The Landsat data archive is one such tool, having documented 48 years of Earth's changing land surface since 1972 and has supported many land cover related research at 30-m resolution (Dong et al., 2016; Phiri and Morgenroth, 2017; Wulder et al., 2019). Recent advancements in cloud-computing platforms and their accessibility, such as the Google Earth Engine (GEE), allow for the archival of large earth observation datasets and provide start-of-art computing power and efficient algorithms for processing data, which allows researchers to quickly map and monitor land cover changes (Wang et al., 2020b). However, the mapping of green fodder using satellite remote sensing has not yet been conducted, let alone analyses of its historical spatiotemporal dynamics. Previous studies about crop mapping and classification have mostly focused on cereal crops and economical crops such as rice, corn, wheat, barley, and soybean (Dong et al., 2016; Gao et al., 2017; Griffiths et al., 2019; Wardlow and Egbert, 2008; Xiao et al., 2005b; Zhong et al., 2014). Those efforts on crop mapping, including the application of time series Landsat imagery and phenology information, are important references for mapping green fodder (Gao et al., 2017; Zhang et al., 2015b).

Several studies have adopted phenological metrics as input to train the classifiers in decision tree classification algorithms for crop mapping, including paddy rice, corn, and soybean (Zhang et al., 2015a; Zhong et al., 2014). Most of the existing phenology-based classification algorithms identify and make use of the special phenological characteristics in critical time windows to separate the target land cover type from other land cover types. For example, pixel- and phenology-based algorithms have been applied to paddy rice mapping by capturing the irrigation signal during the rice transplanting phase (Zhang et al., 2015a; Zhou et al., 2016), red cedar mapping by using evergreen characteristics during winter (Wang et al., 2017), canola mapping by identifying vegetation characteristics during the flowering phase (Ashourloo et al., 2019). Of particular interest here, green fodder is usually harvested at the early heading stage before full maturity to maximize nutrient retention and maintain palatability (Jacobs and Ward, 2012, 2013). Thus, we hypothesized that the unique phenological characteristics of green fodder could be detected using the pixel- and phenology-based mapping strategy.

Our objective was to map green fodder and analyze the spatio-temporal dynamics of green fodder in northeastern TP over the past decade (2010–2019). Here, we used all the available Landsat images and the Google Earth Engine (GEE) platform to: (1) develop a green fodder index and a pixel- and phenology-based algorithm to map green fodder based on Landsat time series analysis; (2) quantify the spatio-temporal dynamics of green fodder over the past decade using historical Landsat observations; and (3) analyze the land sources for green fodder expansion.

2. Material and methods

2.1. Study area

Our study area (34°38′–36°8′N, 100°7′–102°7′E) was in the northeastern TP with an area of 17,902 km^2, covering Guinan, Tongde, and Zeku Counties in Qinghai Province, China. Tongde and Zeku Counties are situated in the northeastern corner of the Three-River Headwaters Region (TRHR), which is the cradle of the Yangtze River, Yellow River, and Lancang River. This area is the most biodiverse high-altitude nature reserve in the world and is known as "China's Water Tower". The study area has a plateau continental climate, with an annual mean air temperature of around 2.0 °C and average precipitation of approximately 450 mm, which mainly falls during the summer monsoon. Meteorological disasters, such as cold damage, snow, and hail, frequently threaten agriculture and animal husbandry. The average altitude of the study area is 3605 m, ranging from 2222 m to 5011 m.

Croplands and grasslands are the major land cover types in the study area. Croplands are mostly distributed in the areas with relatively flat terrain, which mainly lie in two regions: central and southern Guinan County and northern Tongde County (Fig. 1). Fodder oat and fodder rapeseed are the main green fodder crops in this region, and both of them are planted and harvested during similar windows of time (Abdelraheem et al., 2019; Council, 1992; Li et al., 2020; Lithourgidis et al., 2006; Qin, 2004; Wang et al., 2016; Zhang et al., 1998). Fodder oat is usually harvested in the mid to late growing season as green fodder, while fodder rapeseed is usually harvested between the bolting and flowering stages (Wang et al., 2015; Yang et al., 2018). The timing of the fodder oat planting and harvest allows the crop to can better adapt to the light, and temperature, and precipitation conditions in the alpine pastoral area and to obtain high, good quality yields (Zhang et al., 1998). Fodder rapeseed stems, which are abundant in organic matter, crude protein, and dry matter, is usually harvested between the bolting and flowering stages as rough forage (Wang et al., 2016; Yang et al., 2018).

2.2. Data

2.2.1. Time series Landsat data and pre-processing

All the available Landsat images from 2009 to 2019 were used for tracking green fodder, including Landsat 5 (2009 to 2011), Landsat 7 (2009 to 2019), and Landsat 8 (2013–2019). The study area covers five path/rows of Landsat images (132/35, 132/36, 133/35, 133/36, and 131/36). We established a two-dimensional matrix to estimate the data volume and quality of all the Landsat land surface reflectance data since 2009 by Landsat path/row and by the main growing season (Fig. 2). The numbers in the matrix represent all the observations of a certain image or a month in a certain year, regardless of the interference of clouds, snow, and cloud shadow. All the data processing was conducted in the Google Earth Engine (GEE) platform, which has been widely used for pixel-based land cover classification and crop mapping (Shelestov et al., 2017). The codes used for data preprocessing and analyses are available here (https://github.com/tessieblink/GreenFodderMapping.git).

The data volume and data quality of good observations for individual pixels were assessed. Clouds and shadows are the main sources of noise and reduce the volume of useful data (Zhu and Woodcock, 2012). Also, the Landsat 7 ETM + scan line corrector (SLC) failed on May 31, 2003, causing wedge-shaped scan-to-scan gaps in the images and a loss of approximately 22% of the pixels (Scaramuzza and Barsi, 2005). Landsat data volume has increased since 2013 with the launch of Landsat 8. We

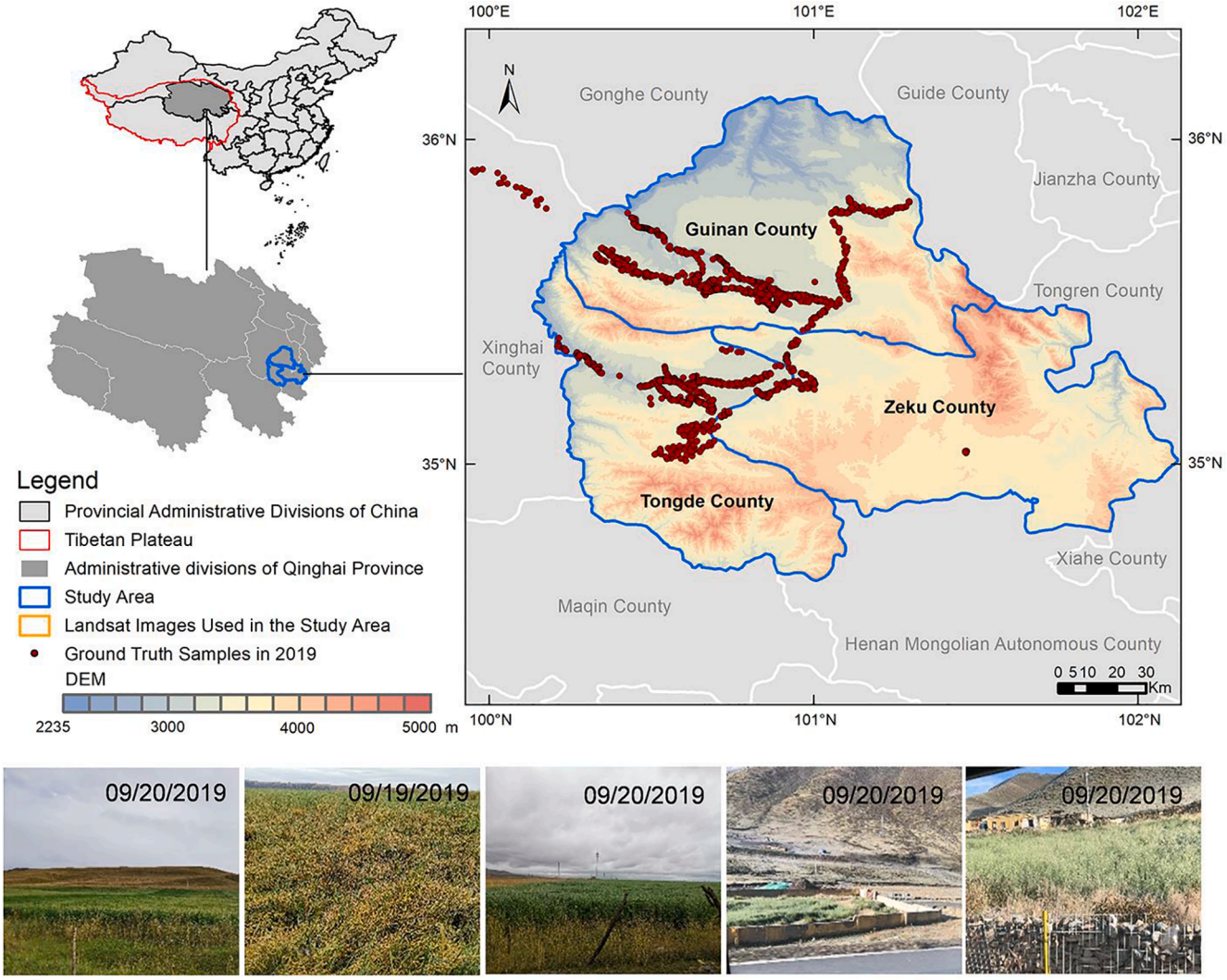

Fig. 1. Location of the study area and ground survey photographs. The location of the study in Qinghai Province, China, is shown in the left figure, where the Landsat images used in our study are with yellow rectangles. The right figure shows the digital elevation model (DEM) of the study area, the three studied counties, and the locations of field samples in 2019. At the bottom of the figure, some field photos of green fodder fields are shown. The base map of DEM dataset at 90 m resolution is from Resource and Environment Science and Data Center (http://www.resdc.cn/) of Chinese Academy of Sciences.

counted the number of good Landsat 5/7/8 pixels in the beginning and end months of the growing season (June and September) for each year from 2009 to 2019 (Fig. S1). For each year, about 2% of the pixels in the study area did not have any good observations in June and September, particularly for 2010 and 2012 when the percentage of pixels with zero observations was higher (Fig. 3). Therefore, retrospective analysis and continuous monitoring of land cover dynamics are attainable at least with a time interval of two years or more in the Tibetan Plateau (Fig.S2) (Zhou et al., 2019).

Multi-sensor image compositing is an important approach for pixel-level time series data analyses (Griffiths et al., 2019). The TM, ETM+, and OLI instrument data are closely related and can easily be consolidated into one continuous record to reduce the number of missing observations from ETM + SLC-off gaps and cloud/shadow masking. Thus, we harmonized all the Landsat 5/7/8 surface reflectance data available between April 2009 and October 2019 for our study area within the GEE platform. The harmonization algorithm used the OLS regression coefficients to harmonize TM/ETM + to OLI, because TM/ETM + has a different spectral band setting from OLI (Roy et al., 2016). Then we removed the cloud/shadow pixels using the CFmask (Zhu et al., 2015). Also, we used a composite of the images from the previous year, current year, and subsequent year as the input data for a certain epoch (Baumann et al., 2017; Flood, 2013). For example, if the target year was 2015, then the actual input data was the image collection from April 2014 to October 2016.

A normalized differenced index is less susceptible to effects caused by land cover changes, such as sun-sensor geometry and bidirectional reflectance distribution (Gu et al., 2013). We computed three common vegetation indices (VIs) using good observations from the Landsat surface reflectance data. They were the Normalized Difference Vegetation Index (NDVI) (Joshi et al., 2016; Tucker, 1979), Enhanced Vegetation Index (EVI) (Huete et al., 2002), and Land Surface Water Index (LSWI) (Dong et al., 2016; Tucker, 1979; Wang et al., 2017; Xiao et al., 2005a; Xiao et al., 2005b) (Eq. 1–3). NDVI and EVI represent vegetation greening, while LSWI is sensitive to equivalent water thickness because the SWIR band is sensitive to a leaf water content of vegetation and soil moisture (Xiao et al., 2006). These VIs provide information on vegetation growth stage and state. The three vegetation indices were calculated using the following equations:

$$\mathrm{NDVI} = \frac{\rho_{nir} - \rho_{\mathrm{red}}}{\rho_{nir} + \rho_{\mathrm{red}}} \quad (1)$$

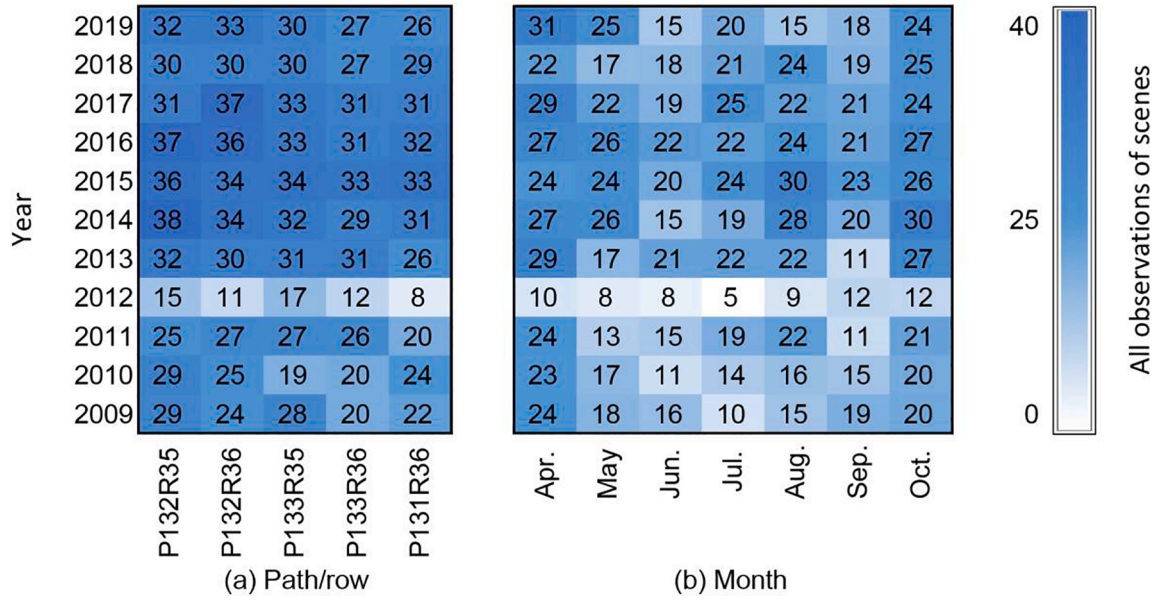

Fig. 2. The annual distribution of all Landsat scenes from 2009 to 2019. Statistics were conducted by (a) path/row and (b) month. The statistics of all Landsat observations for every path/row include the main growing season from April to October. And the statistics of all Landsat observations for every month contains all the path/row covering our study area.

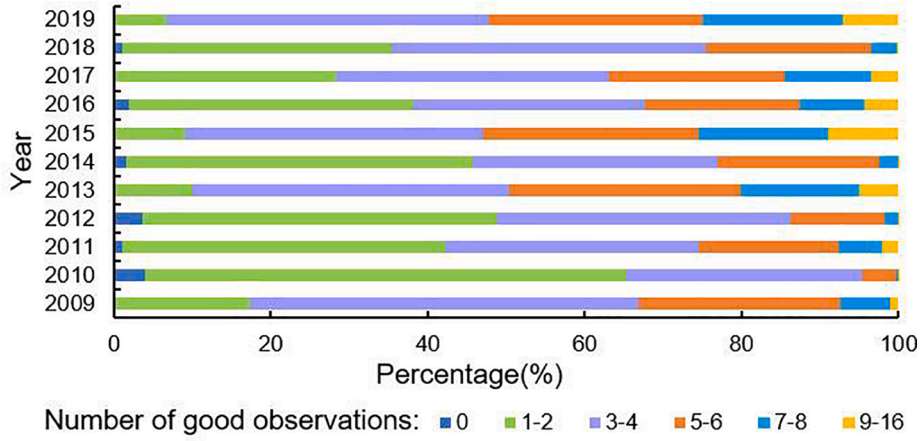

Fig. 3. Percentage of good observations in June and September from 2009 to 2019.

$$\mathrm{EVI} = 2.5 \times \frac{\rho_{nir} - \rho_{\mathrm{red}}}{\rho_{nir} + 6 \times \rho_{\mathrm{red}} - 7.5 \times \rho_{\mathrm{blue}} + 1} \quad (2)$$

$$\mathrm{LSWI} = \frac{\rho_{nir} - \rho_{swir}}{\rho_{nir} + \rho_{swir}} \quad (3)$$

where ρ_{blue}, ρ_{red}, ρ_{nir}, and ρ_{swir} are the surface reflectance values of the blue (450–520 nm/452–512 nm), red (630–690 nm/636–673 nm), near-infrared (770–900 nm/851–879 nm), and shortwave infrared bands (1550–1750 nm/1556–1651 nm) from the TM/ETM + or OLI sensor.

2.2.2. Field survey data

We conducted a field survey during September 2019 to collect ground truth data for mapping green fodders. We took photos and recorded their location and land cover types using the OvitalMap software and mobile devices, which integrated GPS positioning and multi-source map data synthesis. The ground truth samples mainly focused on green fodder (oat and rapeseed), grain crops (barley and other crops), artificial grassland crops (mainly *Elymus* sp.) and other natural vegetation (natural pasture and woodlands). We supplemented the woodland, grassland, construction land, and water sample points by visual interpretation using the Google Earth high-resolution composite imagery. The final ground truth sample collection consisted of 1307 sample points collected from field trips and in-house visual interpretation (Fig. S3), including 146 green fodder samples (11%), and 1161 samples of other land cover types (89%). We randomly divided the point collection into two subsets using a 1:1 ratio for training and validating. The training regions of interest (ROIs) were digitalized manually based on the training points according to the field photos and Google Earth images to reduce the intragroup differences in pixels of the same land cover type. In the end, we got training ROIs with plots/pixels of 48 ROIs/12153 pixels for green fodder, 241 ROIs/73581 pixels for other non-green fodder vegetation, 45 ROIs/144 pixels for water, and 43 ROIs/2317 pixels for built-up land in 2019.

2.2.3. Other data

The China's Land Use/Cover Datasets (CLUDs) from Resource and Environment Science and Data Center (http://www.resdc.cn/) of the Chinese Academy of Sciences were used to figure out land sources where green fodder crops were planted in this study. The multi-temporal CLUD

maps at 100 m resolution were generated by human–computer interactive interpretation method based on Landsat images from the 1980s to 2015 with 5-year intervals and high accuracy (Dong et al., 2015; Liu et al., 2014). Here we extracted the land cover maps in Tibetan Plateau in 2010 and 2015 for analyzing land cover source of newly cultivated green fodder.

Besides, we use high-resolution images of Google Earth as auxiliary data to help construct completed sample sets and inspect the growth status of green fodder crops.

2.3. Methods

We developed a pixel- and phenology-based approach to map green fodder (Fig. 4). First, we produced a long-term time series of NDVI, EVI, and LSWI of the training ROIs to analyze phenological characteristics of various land cover types using a harmonized Landsat 5/7/8 surface reflectance dataset and ground truth data in 2019. Then we created a green-fodder index and used it to map pixel-based green fodder in 2019. The historical green fodder maps for 2010 and 2015 were produced by transferring the pixel- and phenology-based algorithm to describe the dynamics of green fodder in the study area. Finally, the performance of the green fodder maps in each period was evaluated using the validation sample points, which were collected via field survey and by using Google Earth images from 2009 to 2019. We also compared China's Land-Use/Cover Datasets (CLUDs) in 2010 and 2015 to our green fodder maps for further analysis on land sources of green fodder expansion.

2.3.1. Phenology and signature analysis of green fodders

We randomly selected nine sites covered with oat, rapeseed, barley, other crops, *Elymus* sp., grassland, woodland, water, and buildings according to the field photos and landscapes from Google Earth images (Fig. S4, 5). The grassland refers to natural pasture with traditional grazing activities. The time-series NDVI, EVI, and LSWI at these sites using the harmonized Landsat dataset in 2019 are shown in Fig. 5. The vegetation index time series of built-up lands usually does not fluctuate because of the very low vegetation cover, as shown in Fig. S6.

We found that the green fodder crops are planted and green up later than other vegetation types. Green fodder crops are harvested at the early heading stage when the vegetation has high water content and bright green stems and ears, while other crops are harvested after full maturity when the plant water content is low, and the crop has lost chlorophyll. These differences in the planting and harvest time of green fodder allow us to separate green fodder from other vegetation. In this region, green fodder (mainly oat and rapeseed) is harvested halfway through its growth period with the most vigorous growth, when other crop types are harvested at the end of their growing season. Thus, there is an obvious difference in the time series vegetation indices for green fodder and other vegetation (Fig. 5). The most significant difference was in the beginning (June) and the end (September) of the growing season. The VIs for green fodder peaked in September while the VIs for other vegetation types peaked a month or two sooner, which may facilitate separating green fodder from other land cover types. Non-vegetation land cover types, such as water and built-up lands, had the lowest VIs and no obvious seasonal fluctuation compared to green fodder and other vegetation (Fig. 5, Fig. S6).

The multiple temporal RGB images of the green fodder field also showed the different growing stages from April to October (Fig. 6a-h). Green fodder fields look like bare ground before June but dark green in

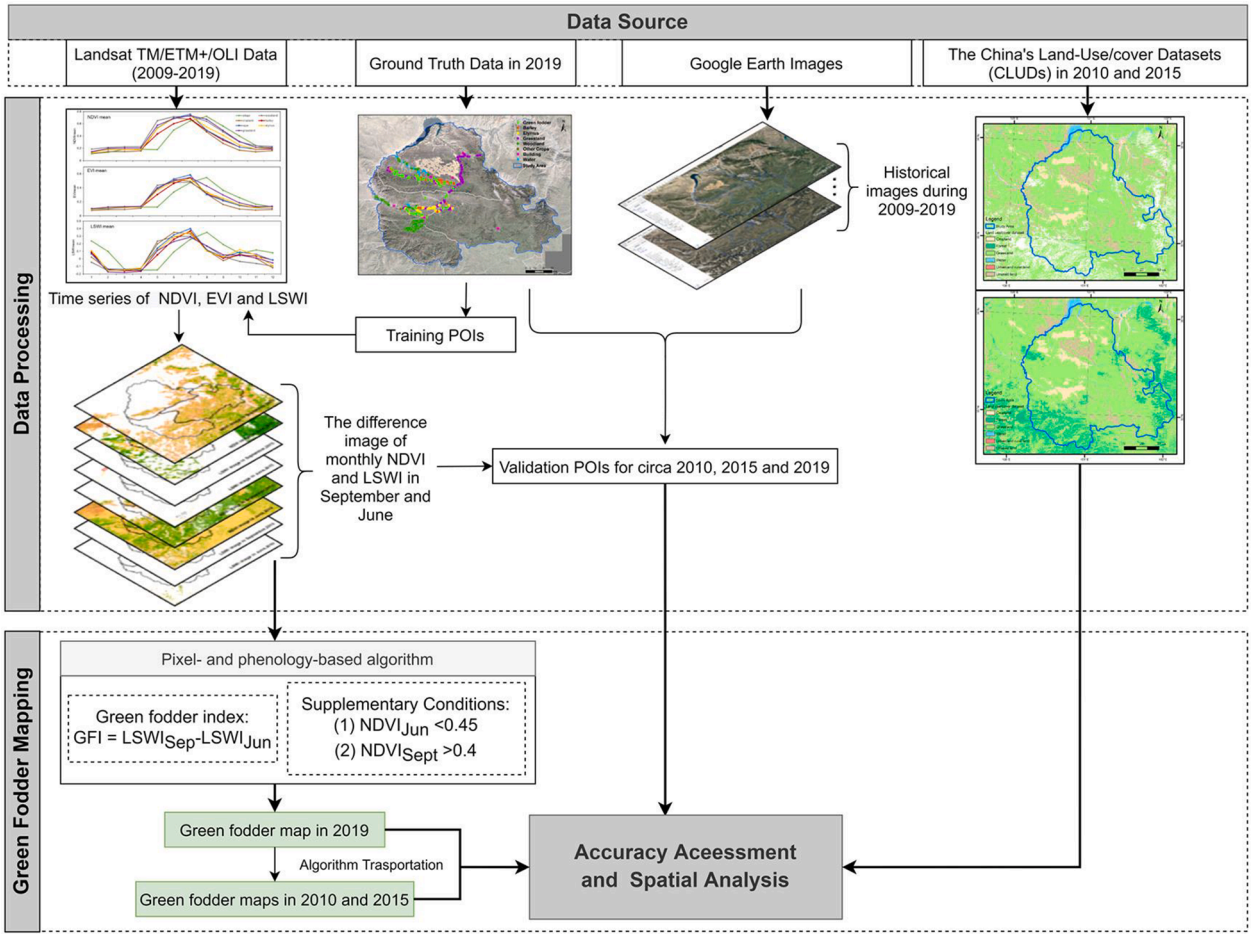

Fig. 4. Flowchart of green fodder mapping and analysis method.

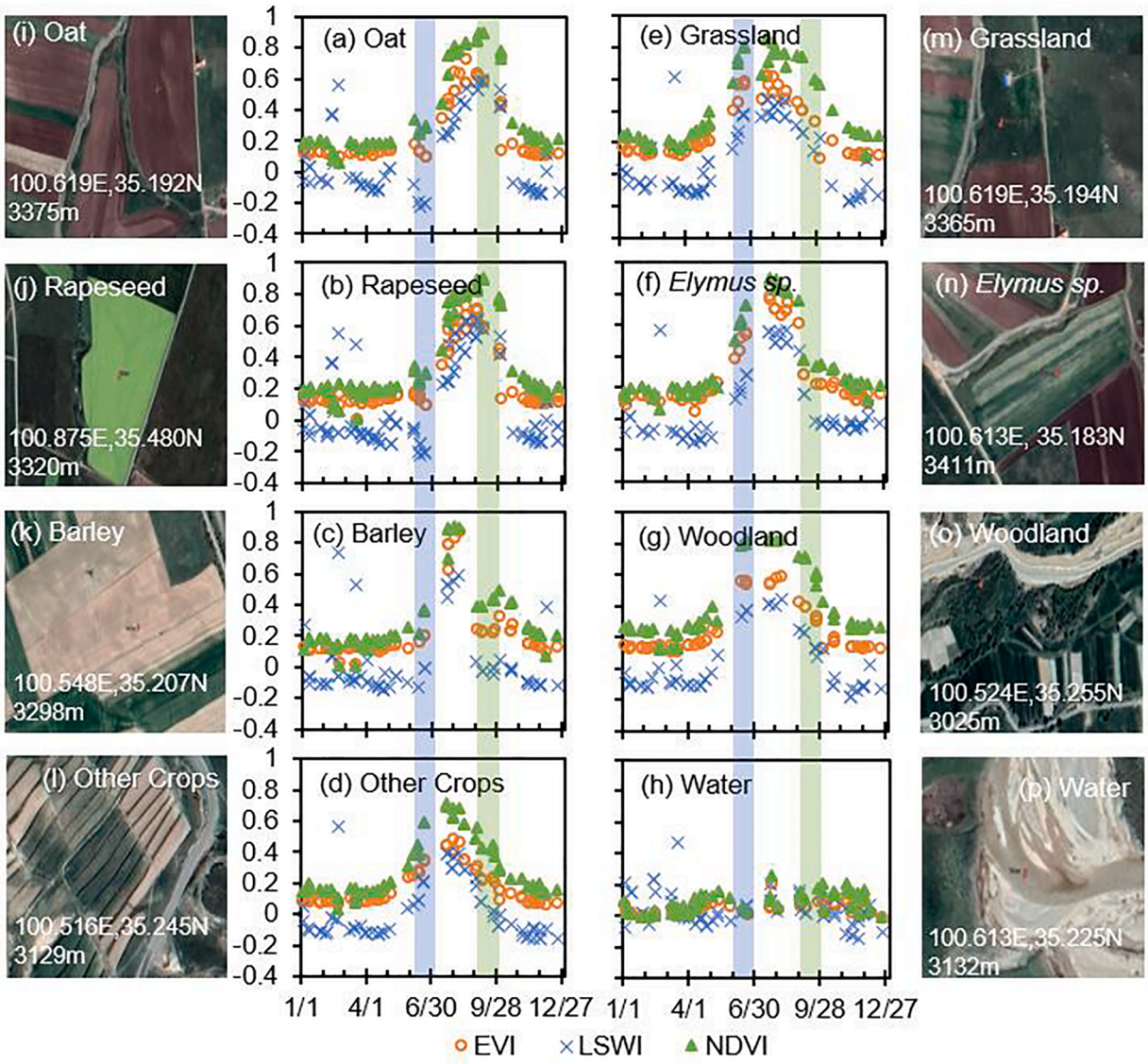

Fig. 5. The Landsat-derived time-series NDVI, EVI, and LSWI in 2019 for main land cover types. (a-h) are time series charts of oat, rapeseed, barley, other crops, grassland, *Elymus* sp., woodland and water. The blue and green bars mark vegetation index values in June and September, respectively. Green fodder crops mainly include oat and rapeseed in the study area. The barley is the main cereal crops in this region. *Elymus* sp. is the main artificial grassland. (i-p) are zoom-in landscapes and locations of these main land cover types.

September. The NDVI and LSWI in June and September corroborated these observations (Fig. 6i-l).

2.3.2. *Green fodder mapping*

Given the unique phenological characteristics of green fodder, we developed a pixel- and phenology-based algorithm for mapping green fodder by using the difference in VIs values between green fodder and other vegetation at the beginning and end of the growing season. To reduce the impact of insufficient data and poor data quality, we used the multi-sensor harmonization data as input.

First, we calculated the monthly average of the VIs for individual pixels making full use of all the available Landsat land surface reflectance data over 2017–2019. Then we produced a histogram of the difference between the monthly mean values of VIs in September and in June ($NDVI_{Sep\text{-}Jun}$, $EVI_{Sep\text{-}Jun}$, and $LSWI_{Sep\text{-}Jun}$) and their standard deviations (Fig. 7). The comparison suggested that the three VIs have the potential to separate green fodder from other land cover types. Then we adjusted the error bars to twice the standard deviation to determine the optimal index, and we found that $LSWI_{Sep\text{-}Jun}$ was the best indicator to discriminate between green fodder and other vegetation cover types. These results also suggested that the $LSWI_{Sep\text{-}Jun}$ threshold of 0.3 may be possible to extract the green fodder (Fig. 7b). Probability analysis showed that using a threshold of 0.3 can achieve a confidence interval of 95%.

However, the high $LSWI_{Sep\text{-}Jun}$ could result from snowmelt in spring and rain or snow accumulation in fall (Boles et al., 2004), and the phenology features in critical time windows could also be true for other land cover types, such as swamp or wetland. So we added NDVI thresholds in June and September to offset the inherent disadvantage of LSWI and enhance the difference between green fodder and other land covers.

In summary, we first developed a green fodder index (GFI, Eq. 4) using the Landsat-derived monthly time series LSWI in 2019, then produced the green fodder map at a regional scale in 2019 using the innovative green fodder index and two additional supplementary conditions: (1) green fodder index > 0.3, (2) $NDVI_{June} < 0.45$ and (3) $NDVI_{Sep} > 0.4$ (Fig. 8). Then we generated two historical green fodder maps in 2010 and 2015 using the same algorithm. At each period, we

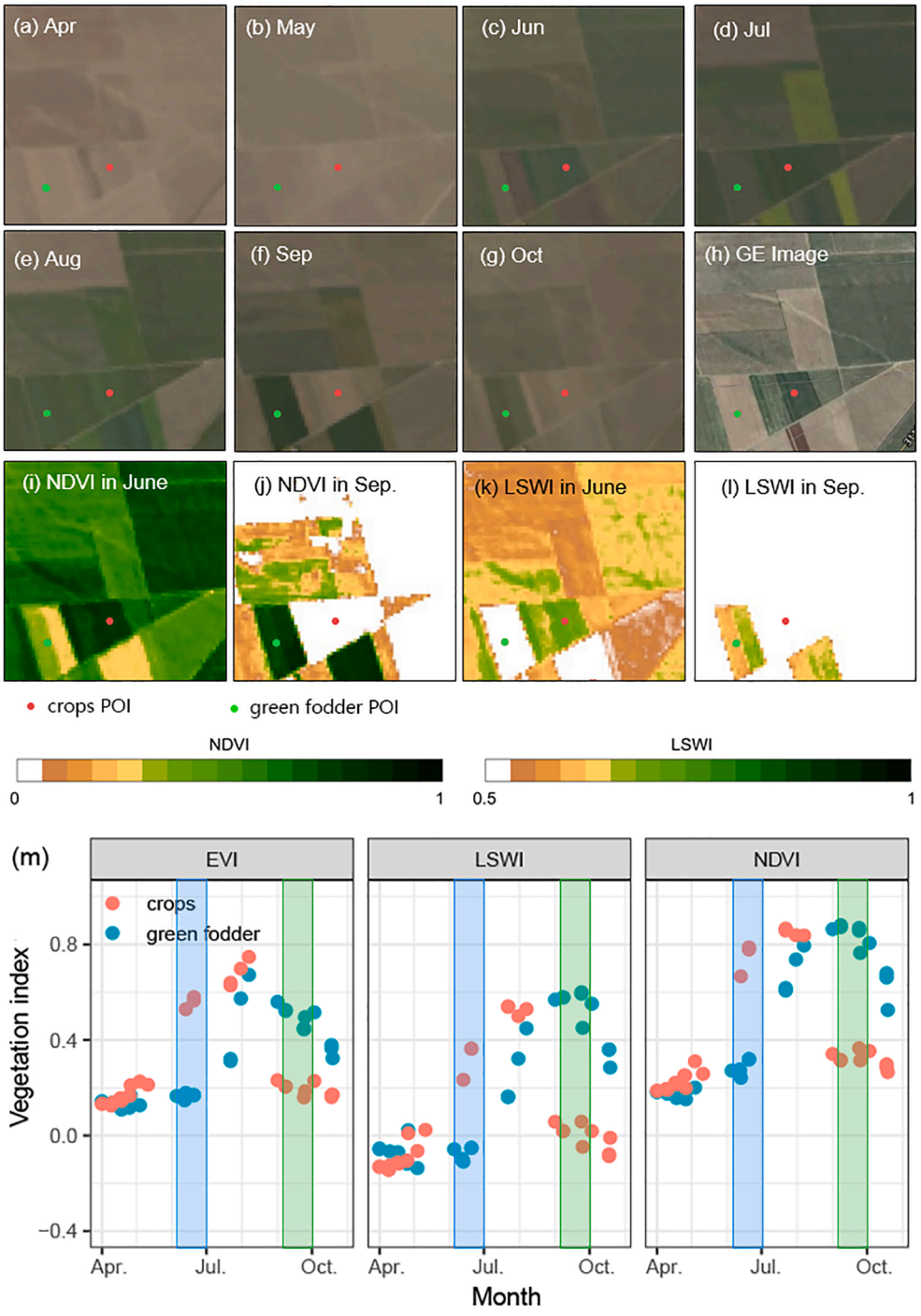

Fig. 6. Landsat-derived true color images during the growing season and a Google Earth composite image of typical green fodder and cropland points of interest marked with bright green and red points. (a-g) are true-color images from April to October. (h) is the latest Google Earth composite image shot on June 2019. (i-m) are NDVI and LSWI images in June and in September. (m) shows the time series chart of the green fodder and crop points of interest during the main growing season (April to October). The blue and green bars in Fig. 6 (m) showed the vegetation index values of June and September, respectively.

counted the number of individual pixels labeled green fodder and non-green fodder and calculated the area of each category for change analyses.

$$GFI = LSWI_{Sep} - LSWI_{Jun} \quad (4)$$

2.3.3. Accuracy assessment

We adopted a quantitative stratified random sampling design to collect validation sample points to evaluate the accuracies of historical green fodder maps. It is best for the sample size allocated to each stratum to be proportional to the area of the stratum and slightly increasing the sample size of rare classes can balance the interaction between the user, producer, and overall accuracy (Olofsson et al., 2014). We stratified two strata of green fodder and other land cover types, collected validation sample points using the corresponding high-resolution images from Google Earth and Landsat-derived NDVI and LSWI images in the early and late growing season (Fig. 6). Green fodder occupied much smaller areas than other land cover types (Fig. S7), so we slightly increased the quantitative proportion of green fodder sample points for the maps in two historical periods. As a result, we collected 310 validation POIs for 2010, 306 for 2015, and 585 for 2019, and the proportions of green fodder were 20%, 19%, and 12% respectively. The number of validation sample points in various land cover classes was shown in Table S1 and the spatial distribution of validation sample points was shown in Fig. S3b and Fig. S8.

We calculated the overall accuracies (OA), user's accuracies (UA),

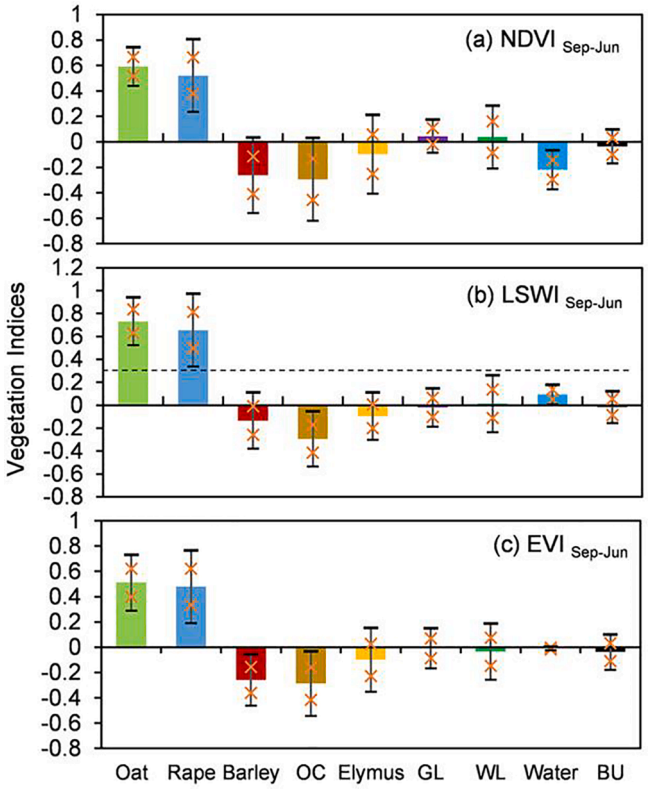

Fig. 7. The mean value, standard deviation (SD), and twice the SD of the difference between monthly mean values of NDVI ($NDVI_{Sep-Jun}$, a), LSWI ($LSWI_{Sep-Jun}$, b), and EVI ($EVI_{Sep-Jun}$, c) in September and in June. The vertical bars in different colors represent the mean value of indices of different land cover types. OC, GL, WL, and BU are abbreviations for other crops, grassland, woodland, and built-up land, respectively. On each mean value bar, the orange cross marked the corresponding SD and the black dash marked twice the SD.

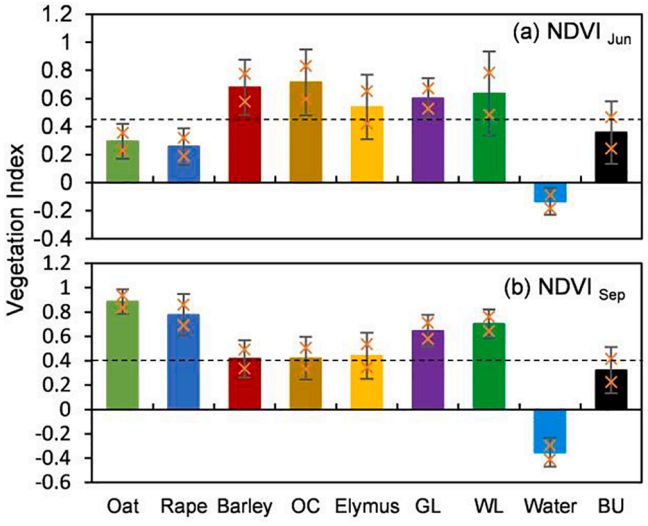

Fig. 8. The mean value, standard deviation (SD), and twice the SD of NDVI in June ($NDVI_{Jun}$, a) and NDVI in September ($NDVI_{Sep}$, b) for different land cover type. The vertical bars in different colors represent the mean value of indices of various land cover types. OC, GL, WL, and BU are abbreviations for other crops, grassland, woodland, and built-up land, respectively. On each mean value bar, the orange cross marked the corresponding SD and the black dash marked twice the SD.

producer's accuracies (PA), and Matthews correlation coefficients (MCC) of our green fodder maps in each period. MCC (Eq. 5) is an alternative measure for F1-score or Cohen's kappa and overcomes issues related to imbalanced datasets, and thus MCC better describes the accuracy of the binary classification model (Chicco and Jurman, 2020). MCC is calculated based on the standard confusion matrix (Table S2).

$$MCC = \frac{tp \times tn - fp \times fn}{\sqrt{tp + fp \times (tp + fn) \times (tn + fp) \times (tn + fn)}} \quad (5)$$

(worst value: -1; best value: +1)

2.3.4. Spatiotemporal pattern of green fodder expansion and its source analyses

The sources of newly reclaimed green fodders were analyzed based on green fodder maps produced in this study and China's Land Use/Cover Datasets (CLUDs). We first overlaid green fodder maps in 2010, 2015, and 2019 to get the land pixels with green fodder expansion during the two periods (2010–2015, 2015–2019). Then the newly green fodder cultivation areas in these two periods were overlaid with CLUDs in 2010 and 2015, respectively. We calculated areas of different land-use types within the newly reclaimed green fodder pixels and conducted a trace analysis of the new green fodder expansion. The green fodder abandonment also existed but with a very limited area (neglectable comparing to green fodder expansion), thus the conversions from green fodders to the other land types were not considered here.

3. Results

3.1. Accuracy assessment of green fodder maps

We mapped green fodder in 2010, 2015, and 2019 over the past decade. Accuracy assessment for the resultant maps was conducted using the validation sample points introduced in Section 2.3.3 The accuracy assessment results suggested that the green fodder maps had reasonably high accuracies, as can be seen from Table 1. The overall accuracies (OA) were 94.2%, 93.1%, and 96.6%, the MCCs were 0.81, 0.76, and 0.83 in 2010, 2015, and 2019, respectively. Overall, our results indicated that the green fodder maps in these three periods had reasonably high accuracies and can be used to track the dynamics of

Table 1
Accuracy assessment of green fodder maps in 2010, 2015, and 2019 based on the ground truth samples.

Periods		Ground truth pixels		Classified pixels	User accuracy (UA)
		Green fodder	Non-green fodder		
2010	Green fodder	45	1	46	97.8%
	Non green fodder	17	247	264	93.6%
	Ground truth pixels	62	248	310	OA = 94.2%
	Producer accuracy (PA)	72.6%	99.6%		MCC = 0.81
2015	Green fodder	37	1	38	97.4%
	Non green fodder	20	248	268	92.5%
	Ground truth pixels	57	249	306	OA = 93.1%
	Producer accuracy (PA)	64.9%	99.6%		MCC = 0.76
2019	Green fodder	56	6	62	90.3%
	Non green fodder	14	508	522	97.3%
	Ground truth pixels	70	514	584	OA = 96.6%
	Producer accuracy (PA)	80.0%	98.8%		MCC = 0.83

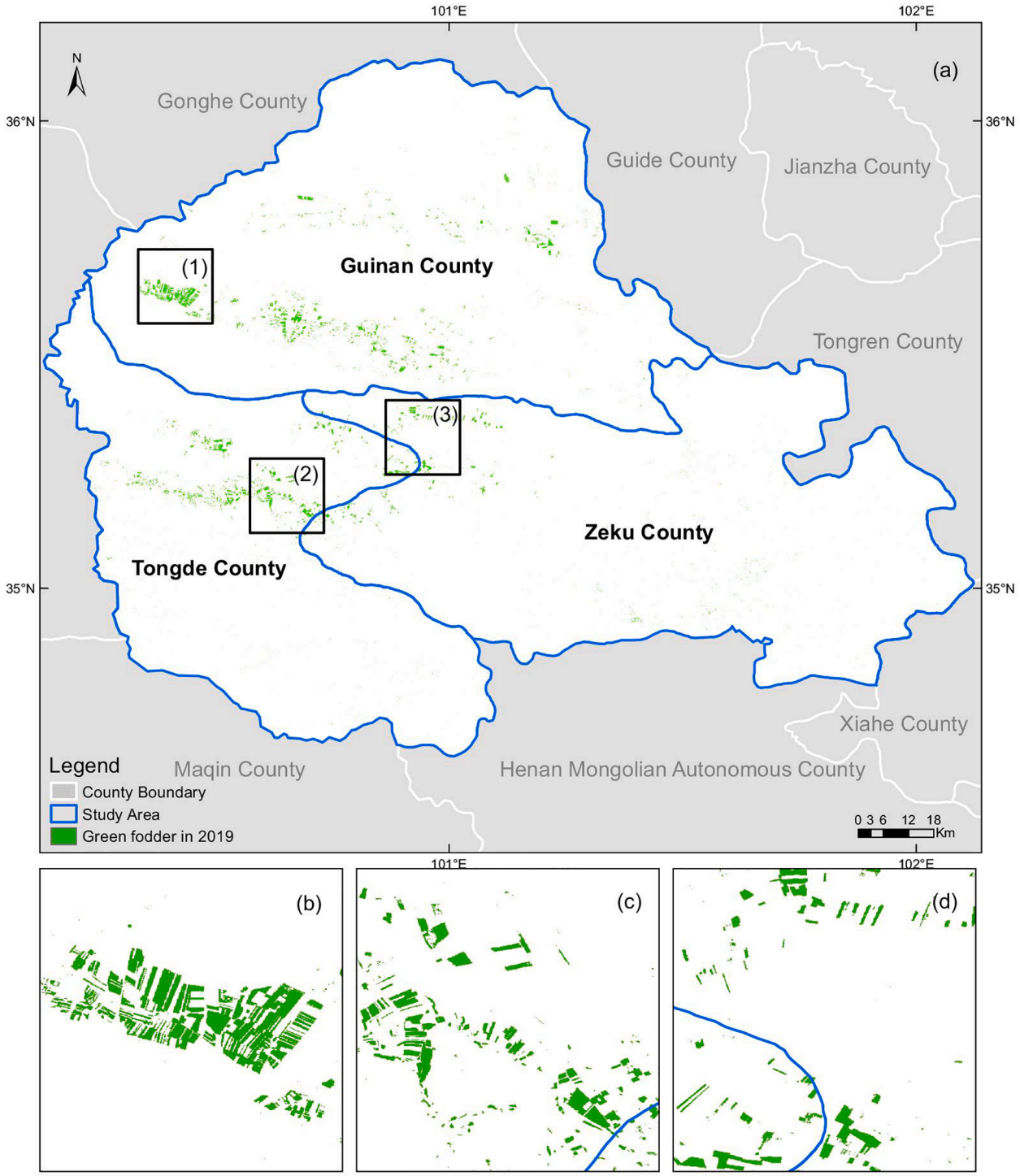

Fig. 9. Spatial distribution of green fodder crops in the study area in 2019. (b-d) are the detailed spatial distributions of green fodder in local regions labeled as 1, 2, and 3 in (a), respectively.

green fodder over the past decade. Fig. 9 shows the spatial distribution of green fodder in 2019.

3.2. Spatial and temporal pattern of green fodder expansion

Green fodder has dramatically expanded in the northeastern TP from 16.26 km^2 in 2010 to 136.09 km^2 in 2019, by 119.83 km^2 during the decade (Fig. 10). In 2010, there were only 16.26 km^2 of green fodder in our study area, mainly located in Tongde and Zeku. The green fodder area increased 2.5 times to 57.48 km^2 in 2015. In Tongde County, the green fodder area increased from 6.23 km^2 in 2010 to 34.24 km^2 in 2015, which was the greatest change among the three counties. In Guinan and Zeku Counties, the green fodder area increased from 3.93 km^2 to 13.38 km^2 and from 6.1 km^2 to 9.86 km^2, respectively. After 2015, the area of green fodder increased by 1.4 times and reached 136.09 km^2 in 2019. During 2015–2019, the expansion of green fodder mainly occurred in Guinan County (56.21 km^2). In Tongde and Zeku Counties, the green fodder area only increased by 10.38 km^2 and 12.02 km^2, respectively (Fig. 10). Throughout the study period (2010–2019), Guinan County accounted for the largest proportion of the region's

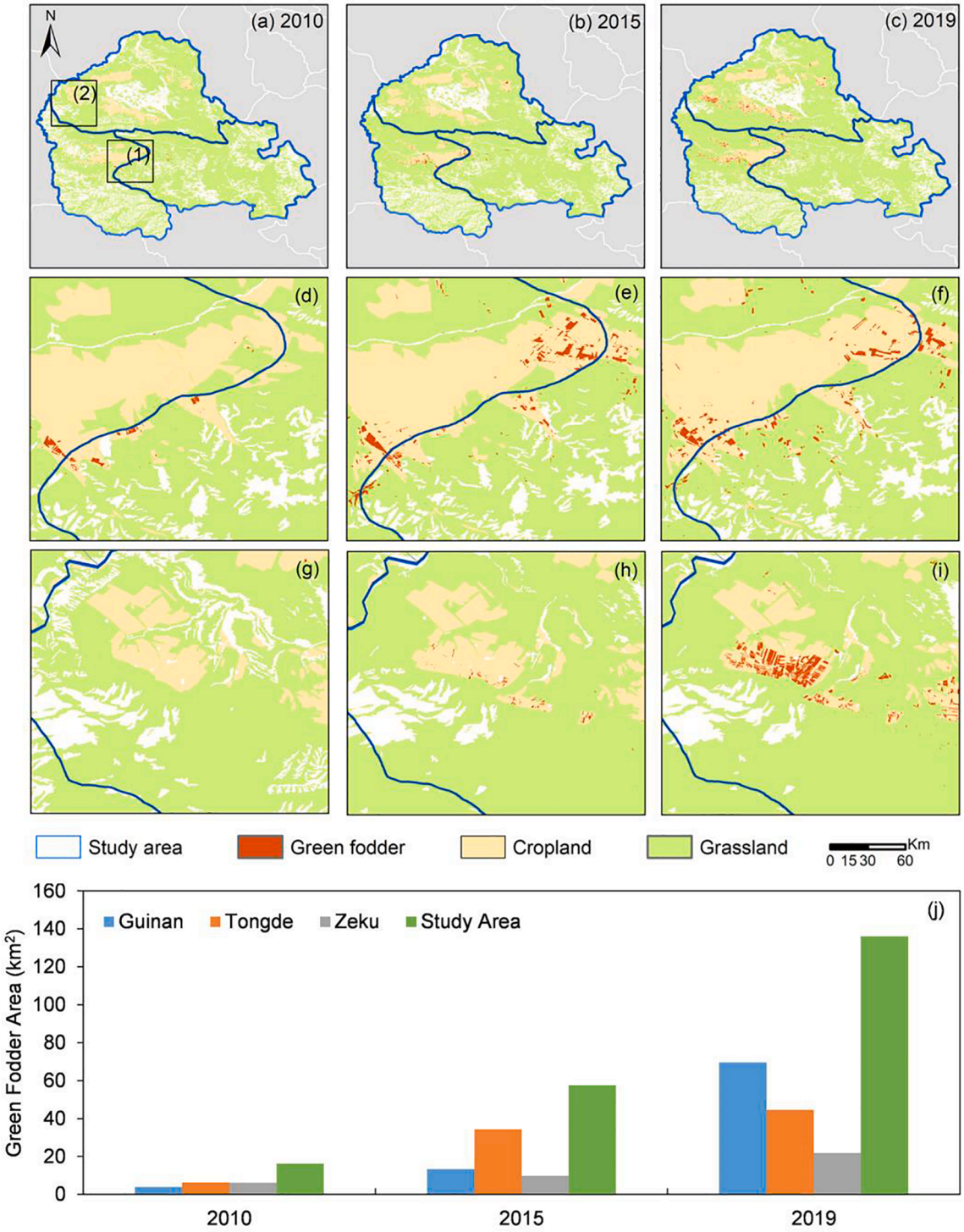

Fig. 10. The historical green fodder maps in the three epochs with two hotspot zoom-in views over three periods (2010, 2015, and 2019). (a-c) are green fodder maps in 2010, 2015, and 2019 and two hot spot regions were labeled as 1 and 2 in (a). (d-i) showed the zoom-in views of hot spots 1 and 2 in 2010 (d, g), 2015 (e, h), and 2019 (f, i). The base map showed the distribution of cropland and grassland extracted China's Land Use/Cover Datasets (CLUDs) in the corresponding year. (j) shows green fodder areas in the three counties and the entire study area in three epochs. The colors of the bars represent green fodder areas in different regions.

increase (54.8% and 65.66 km^2), followed by Tongde County with an increase of 32% and 38.39 km^2.

Spatially, green fodders was sporadically distributed across the main agropastoral areas in this region, including Southern Guinan County, Northern Tongde County, and Western Zeku County. According to the resultant green fodder maps and our field survey, the green fodder planting areas usually occur in two forms. One is the agropastoral ecotone with large-scale planting, the other is scattered small fields planted by nomads close to the nomadic temporary house and roads. From 2010 to 2015, the spatial expansion conspicuously occurred at the county boundary between Tongde and Zeku Counties (Fig. 10d–e, Fig. S9a). Then from 2015 to 2019, the spatial expansion mainly stretched into Tongde County and the cropland region in southern Guinan County (Fig. 10g–i, Fig. S9b).

3.3. Analyses of land sources for green fodder expansion

Green fodder expanded in our study area (Fig. 10j) and we identified the sources of the newly cultivated green fodder using our green fodder maps and CLUDs during 2010–2015 and 2015–2019. We found that around 97% of the new green fodder fields were converted from croplands and grasslands during 2010–2019 (Fig. 11a). The area of newly cultivated green fodders over 2015–2019 was much larger than in 2010–2015. Also, the area converted from croplands to green fodder was much larger than the area converted from grasslands. During 2010–2015, the proportions of green fodder converted from croplands and grasslands were relatively equal (54.2% for croplands and 43.2% for grasslands). However, the proportion of newly cultivated green fodder area converted from croplands was more than twice the area converted from grasslands during 2015–2019, with nearly 80 km^2 of the new green fodder being converted from croplands, which accounted for 71.2% of the total green fodder expansion (Fig. 11b).

Among the three counties, the land cover type of the lands converted to green fodder varied during the two periods. In Guinan, after 2015, the newly cultivated green fodders were mainly converted from croplands, and the proportion of new green fodder converted from croplands increased from 51% to 82%. Conversely, the proportion of new green fodder converted from grasslands during this time was minor and decreased (Fig. 11b). The area of green fodder converted from croplands and grasslands in Tongde did not change much over the two periods. The proportions of cropland-derived and grassland-derived green fodder area slightly increased and decreased, respectively (Fig. 11c). In Zeku, the newly cultivated green fodder area converted from both croplands and grasslands increased slightly, but both the proportions decreased (Fig. 11d), which might be due to green fodder expansion on unused lands.

4. Discussion

4.1. The pixel- and phenology-based approach for green fodder mapping

We proposed a green fodder index and developed a simple algorithm to generate green fodder maps for three historical periods in the alpine region. To our limited knowledge, our study is the first attempt to map alpine green fodder with a pixel- and phenology-based algorithm at a regional scale. The feasibility of this study benefited from the unique phenology characteristics of the green fodder using all the available Landsat data and the cloud computing platform (GEE). First, the unique phenological features of alpine fodder oat and rapeseed play a critical role in our study. For example, green fodder crops have later green-up date and higher greenness and moisture at the end of the growing season than other crops (Jacobs and Ward, 2013). Thus, green fodder crops can be identified effectively on the start and end of the growing season (Fig. 5). The mapping algorithm based on phenological information provided by satellite image time series can be utilized to map crops without the need to training data (Ashourloo et al., 2018; Ashourloo et al., 2019). Second, for cloudy regions where good quality data is more scarce (Zhou et al., 2019), the harmonization of Landsat 5, 7, and 8 images is especially useful because it increases the frequency of good quality observations (Wulder et al., 2019; Wulder et al., 2012), and allows us the opportunity to employ phenology-based approaches to mapping different vegetation types. The GEE platform not only synchronizes all the Landsat data from USGS and various levels of products but also speeds up the process of accessing and calculating a large amount of satellite imagery (Dong et al., 2016; Shelestov et al., 2017).

While the pixel- and phenology-based approach can be used to track the green fodder expansion in the study area, some uncertainties impeded higher accuracy to some extent. First, mixed pixels prohibit more accurate green fodder crop mapping. For example, to make full use

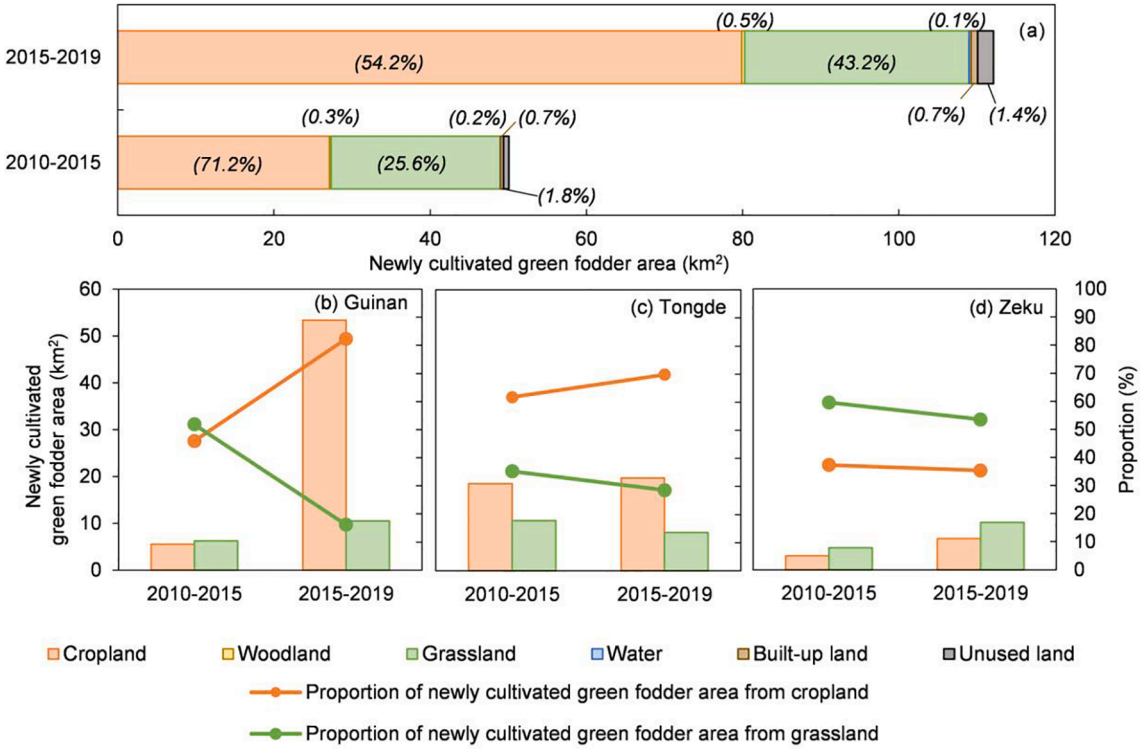

Fig.11. Source pattern of green fodder expansion during 2010–2019. (a) newly cultivated green fodder area from different land cover types in the study area during the two periods of 2010–2015 and 2015–2019. The numeric labels on the bars are the proportion of the newly cultivated green fodder area to the total expansion area in the study area. (b-d) showed the area and proportion of newly cultivated green fodders converted from cropland and grassland during 2010–2015 and 2015–2019 in Guinan, Tongde, and Zeku Counties, respectively. The histograms showed the newly cultivated green fodder area converted from cropland and grassland in different counties, and the line charts showed the proportion of different sources of green fodder expansion to the total fodder area in different counties.

of light energy and improve the palatability of forage, legumes (such as common vetch and alfalfa) are sometimes also intercropped with green fodder (Chen et al., 2015), so it is tremendously difficult to map single green fodder crop when multiple crops are mixed. Also, green fodder is not cultivated in large fields or intensively in smaller fields, and the smallholder production and enclosure planting dominate in the ecotone of agriculture and animal husbandry (De-Qiang, 2003), which could lead to an underestimation of green fodder area (Xiao et al., 2005a). Second, the timing of crop phenology, including the start and end of the growing season and peak photosynthesis, may change over the years due to the interannual variation of preseason temperature and precipitation (Che et al., 2014; Shen et al., 2014; Yang et al., 2019), which may limit the robustness of our algorithm over long-term change detection. Third, the lack of valid satellite observations and the trade-off between spatial and temporal resolutions also hindered the application of the algorithm (Houborg and McCabe, 2018; Zhang et al., 2013b). To reduce these uncertainties, a multi-satellite approach (e.g., using Landsat, Sentinel-1, and Sentinel-2) that takes advantage of finer spatial, temporal, and spectral resolutions of remote sensing observations need to be considered in the future, especially in the regions with a high frequency of cloud and snow cover (Zhou et al., 2019). In the future, we will integrate datasets from multiple sources, such as the Landsat and Sentinel platforms, to improve the robustness of our approach (Sidhu et al., 2018).

4.2. Implications for extensive applications of the proposed approach

Reliable information on green fodder area and its distribution provides important information needed for improving animal husbandry management (Shelestov et al., 2017). Our phenology-based algorithm can be applied in other similar regions, such as the northeastern Tibetan Plateau, where alpine oat and rapeseed serve as the main green fodder crops, or could be used for mapping other green fodder crop species with similar phenological characteristics as alpine fodder oat and rapeseed (Ashourloo et al., 2018; Jin et al., 2019; Velho et al., 2020). For example, the crop calendar in the Tibetan Plateau is consistent because it is constrained by temperature and precipitation, and the growth period is usually from May to September (Zhang et al., 2013a). Silage maize in Iran also has similar phenology in that it is planted relatively late and harvested early (Shahrabi et al., 2020). Our pixel- and phenology algorithm has potential applications in areas with a consistent and stable phenology.

However, due to the importance of phenological features to the algorithm, prior knowledge about crop types, crop calendars, and phenological and/or spectral characteristics by analyzing time series is recommended and some modifications should be considered, such as adjusting the thresholds for other regions or for mapping other green fodder crop species (Wang et al., 2017). The accuracy of phenology-based land cover mapping also depends on the high temporal frequency of satellite images and robust phenology characteristics (Dong et al., 2016). Thus, our approach can be further improved by feature optimization and enhancing observation frequency.

First, the unique phenological features of green fodder we used could be captured by indices other than NDVI, EVI, and LSWI. For instance, normalized differential senescent vegetation index (NDSVI) reflects water content in vegetation when plants begin to age and the leaves turn yellow (Zhong et al., 2014), which could potentially capture the signal of green fodder at the end of the growing season, since green fodder is harvested while, whereas other crops are harvested when fully mature and senescing.

Second, the number of good quality observations within the windows of time that are critical for detecting phenological changes are sometimes far from satisfactory (Fig. 3, Fig. S1). Recently, the accessibility of Sentinel-2 data provides an opportunity to integrate the data with Landsat-8 for better performance in pixel-level land cover mapping due to the higher spatial resolution and more frequent revisit periods of Sentinel-2 (Griffiths et al., 2019; Li and Roy, 2017; Liu et al., 2020; Wang et al., 2020a; Wulder et al., 2019). Spectral information from Sentinel-2 is similar to that from Landsat, which makes it possible to integrate them and helps alleviate the lack of good quality Landsat observations (Li and Roy, 2017). Also, the popularity of the UAV platform has the potential to increase the abundance and flexibility of remote sensing images (Zhao et al., 2020; Zhong et al., 2018). Multi-source data with higher spatial and spectral resolution and a more frequent revisit period could be used in the future to map green fodder with a more optimized algorithm and with higher precision.

4.3. Drivers and consequences of green fodder expansion

We found that green fodder expanded dramatically in northeastern TP over the past decade, which was consistent with a previous study (Deng, 2014), and the expansion of green fodder could be attributed to government policies (Zhai et al., 2019). Initially, fodder crop plantation was encouraged as a part of the national project of 'Returning Grazing to Grassland' (RGG) in 2000, which aimed at pasture restoration through grazing bans, grazing restrictions, fencing rangelands, and promoting fodder cultivation and pen feeding to relieve pastoral land degradation in northern and western China (Hua and Squires, 2015). However, because of the high labor requirements (Garrity and Becker, 1994), it is difficult to implement forage crops in a food crop system without immediate monetary benefit (Devendra and Sevilla, 2002). The Rural Area Forage and Multiple Cropping Forage Grass in Qinghai Province was implemented in 2010, which aimed to promote forage cultivation in food crop areas and increase the income of farmers and herdsmen (Deng, 2014). On a national level, the national Rangeland Ecological Compensation Program (RECP) was first promulgated in 2011 in eight pastoral provinces, including Qinghai Province, to restore pastoral lands, change the production pattern of animal husbandry, and increase herder's incomes (Hua and Squires, 2015). These programs focused on providing various subsidies to herders who were affected by the grazing bans, which included high quality forage seeds, fodders, money subsidies, and other production materials (HOU et al., 2008; Huilan and Yingjun, 2017). The promulgation of the National Plan for Crop Production Structural Adjustment in 2016-2020, which aimed to balance the cultivation areas of grain crops, economic crops and fodder crops was also a key factor affecting the spatial dynamics of the green fodder industry (Ni and Wang, 2019).

Although facing insufficient domestic green fodder supply (Zhai et al., 2019), green fodder cultivation does not always mean a better solution. Green fodder expansion could cause a series of both positive and negative economic and environmental consequences. Green fodder cultivation increased forage production and alleviated grazing pressure by changing other croplands into green fodder croplands, which was an effective nutrient supplement during winter and spring (Council, 1992). Specifically, the production of fodder within food crop systems can reduce soil erosion and ensure feed for sheep, goats, and cattle (Devendra and Sevilla, 2002). Thus, green fodder crops play an important role in promoting the country's sustainable development (Zhai et al., 2019).

According to our analysis, croplands and grasslands were the primary sources for newly cultivated green fodder crops, followed by unused lands (Fig. 11a-b). On the one hand, the land cover change from natural grasslands to green fodder fields results in more land disturbances, including plowing, seeding, and harvesting, which may affect soil water retention capacity, carbon availability, nitrogen and phosphorus cycling, and soil physical and chemical properties (Chen et al., 2010; Li et al., 2020; Ma and Han, 2000). For example, annual planting of oat fodder significantly increased the C and N storage of vegetation but decreased the soil organic carbon and nitrogen in the 0–30 cm soil layer (Wen et al., 2018). In addition, fodder crops can affect carbon dynamics by reducing the respiration intensity compared to natural grasslands used for regular grazing (Zhang et al., 2012).

Activities related to the expansion of green forage production, such

as fertilization and plowing, can also alter biomass allocation in alpine meadows, and create an imbalance between the carbon, nitrogen, and phosphorus cycles on the Tibetan Plateau (Chen et al., 2013; Niu et al., 2009; Niu et al., 2008). Considering the two-sided nature of green fodder expansion, more effective and flexible policy frameworks and agricultural technologies, like crop-forage rotation, should be further studied (Zhai et al., 2019). Yang et al. (2019) found that the timing of peak photosynthesis in alpine grasslands on the Tibetan Plateau is shifting to later in the year. This trend was attributed to preseason soil moisture instead of human activities because human-driven land-use change were not remarkable in the alpine grasslands (Yang et al., 2019). Green fodder is sown and harvested later than other crops, resulting in high greenness in September, but the impacts of green fodder expansion on vegetation phenology and biogeochemical process remain unclear (Niu et al., 2009).

5. Conclusions

The balance between livestock demand and forage supply has deteriorated in the Tibetan Plateau, and the cultivation of forage crops or adopting forage species into crop rotation with highland barley cultivars is an effective way to ease the imbalance between forage supply and animal husbandry. Green fodder has been increasingly cultivated in the northeastern Tibetan Plateau to alleviate the pressure of insufficient animal forage supply during the cold season. The lack of current and historical green fodder maps at a regional scale impedes our understanding of the interaction between the ecological and social-economic systems, as well as the effects of rangeland management and agriculture development planning. Landsat data with 30-m resolution and 16-day revisit cycle has provided consistent observations for over 30 years and an opportunity to trace the dynamics of green fodder. We harmonized all the 858 Landsat TM/ETM+/OLI images to generate the green fodder maps and analyzed the dynamics in the three counties of northeastern Tibetan Plateau using a pixel- and phenology-based algorithm in the Google Earth Engine platform. The phenology characteristics of green fodder were captured by the Landsat-derived time series of vegetation indices, which allowed us to distinguish green fodder from other land cover types. The high accuracy of validation proved the reliability of our algorithm. Based on the remote sensing-based results, we found a remarkable increase in green fodder areas from 2010 to 2019, and croplands and natural grasslands were the two main land sources for green fodder expansion. Our method can be applied to larger regions to better understand the spatial and temporal pattern of green fodder in the Tibetan Plateau and the country, and to determine the causes and consequences of green fodder expansion.

CRediT authorship contribution statement

Tong Yang: Conceptualization, Methodology, Writing - Original Draft, Software, Data Curation, Visualization. **Geli Zhang:** Conceptualization, Writing - review & editing, Supervision, Funding acquisition. **Yuzhe Li:** Investigation, Writing - Review & Editing. **Jiangwen Fan:** Conceptualization, Writing - Review & Editing. **Danfeng Sun:** Writing - Review & Editing. **Jie Wang:** Writing - Review & Editing. **Yuanyuan Di:** Investigation, Writing - Review & Editing. **Nanshan You:** Software, Data curation, Writing - Review & Editing. **Ruoqi Liu:** Writing - Review & Editing. **Qiang Zhang:** Writing - Review & Editing. **Russell B. Doughty:** Writing - Review & Editing.

Declaration of Competing Interest

The authors declare that they have no known competing financial interests or personal relationships that could have appeared to influence the work reported in this paper.

Acknowledgments

This work was supported by the Second Tibetan Plateau of Scientific Expedition and Research Program (2019QZKK0608), the Key Research Program of Frontier Sciences, the Chinese Academy of Sciences (QYZDB-SSW-DQC005), and the 2115 Talent Development Program of China Agricultural University. We thank Prof. Jinwei Dong for his valuable comments in the earlier versions of the manuscript.

Appendix A. Supplementary material

Supplementary data to this article can be found online at https://doi.org/10.1016/j.jag.2021.102394.

References

Abdelraheem, N., Li, F., Guo, P., Sun, Y., Liu, Y., Cheng, Y., Hou, F., 2019. Oat hay as winter feed improves digestibility, nitrogen balance and energy utilization of Tibetan sheep (Ovis aries) in the Qinghai Tibetan Plateau. Livestock Science 230, 103854.

Ashourloo, D., Shahrabi, H., Azadbakht, M., Aghighi, H., Matkan, A., Radiom, S., 2018. A Novel Automatic Method for Alfalfa Mapping Using Time Series of Landsat-8 OLI Data. In: IEEE Journal of Selected Topics in Applied Earth Observations and Remote Sensing PP, pp. 1–10.

Ashourloo, D., Shahrabi, H., Azadbakht, M., Aghighi, H., Nematollahi, H., Alimohammadi, A., Matkan, A., 2019. Automatic canola mapping using time series of Sentinel 2 images. ISPRS J. Photogrammetry Remote Sens. 156, 63–76.

Baumann, M., Ozdogan, M., Richardson, A.D., Radeloff, V.C., 2017. Phenology from Landsat when data is scarce: Using MODIS and Dynamic Time-Warping to combine multi-year Landsat imagery to derive annual phenology curves. Int. J. Appl. Earth Observat. Geoinfo. 54, 72–83.

Boles, S.H., Xiao, X., Liu, J., Zhang, Q., Munkhtuya, S., Chen, S., Ojima, D., 2004. Land cover characterization of Temperate East Asia using multi-temporal VEGETATION sensor data. Remote Sens. Environ. 90, 477–489.

Che, M., Chen, B., Innes, J.L., Wang, G., Dou, X., Zhou, T., Zhang, H., Yan, J., Xu, G., Zhao, H., 2014. Spatial and temporal variations in the end date of the vegetation growing season throughout the Qinghai-Tibetan Plateau from 1982 to 2011. Agri. Forest Meteorol. 189–190, 81–90.

Chen, B., Zhang, X., Tao, J., Wu, J., Wang, J., Shi, P., Zhang, Y., Yu, C., 2014. The impact of climate change and anthropogenic activities on alpine grassland over the Qinghai-Tibet Plateau. Agri. Forest Meteorol. 189–190, 11–18.

Chen, D., Zhang, S., Dong, S., Wang, X., Du, G., 2010. Effect of land-use on soil nutrients and microbial biomass of an alpine region on the northeastern Tibetan plateau, China. Land Degrad. Develop. 21, 446–452.

Chen, H., Zhu, Q., Peng, C., Wu, N., Wang, Y., Fang, X., Gao, Y., Zhu, D., Yang, G., Tian, J., Kang, X., Piao, S., Ouyang, H., Xiang, W., Luo, Z., Jiang, H., Song, X., Zhang, Y., Yu, G., Zhao, X., Gong, P., Yao, T., Wu, J., 2013. The impacts of climate change and human activities on biogeochemical cycles on the Qinghai-Tibetan Plateau. Glob Chang. Biol. 19, 2940–2955.

Chen, L., Guo, G., Yu, C., Zhang, J., Shimojo, M., Shao, T., 2015. The effects of replacement of whole-plant corn with oat and common vetch on the fermentation quality, chemical composition and aerobic stability of total mixed ration silage in T ibet. Animal Sci. J. 86, 69–76.

Chicco, D., Jurman, G., 2020. The advantages of the Matthews correlation coefficient (MCC) over F1 score and accuracy in binary classification evaluation. BMC Genomics 21.

Council, N.R., 1992. Grasslands and Grassland Sciences in Northern China. The National Academies Press, Washington, DC.

De-Qiang, A.I., 2003. The Analysis On Forage Planting Benefit In Qingshui Village, Down Dawu Township Of Maqing County. Qinghai Prataculture.

Deng, Y., 2014. The stand on the development of the rural area forage and multiple cropping forage grass in Qinghai Province. Qinghai Prataculture 23, 46–48.

Devendra, C., Sevilla, C.C., 2002. Availability and use of feed resources in crop–animal systems in Asia. Agri. Syst. 71, 59–73.

Dong, J., Xiao, X., Menarguez, M.A., Zhang, G., Qin, Y., Thau, D., Biradar, C., Moore, B., 2016. Mapping paddy rice planting area in northeastern Asia with Landsat 8 images, phenology-based algorithm and Google Earth Engine. Remote Sensing of Environment, S003442571630044X.

Dong, J.W., Xiao, X.M., Kou, W.L., Qin, Y.W., Zhang, G.L., Li, L., Jin, C., Zhou, Y.T., Wang, J., Biradar, C., 2015. Tracking the dynamics of paddy rice planting area in 1986–2010 through time series Landsat images and phenology-based algorithms. Remote Sens. Environ. 160, 99–113.

Flood, N., 2013. Seasonal composite Landsat TM/ETM+ images using the medoid (a multi-dimensional median). Remote Sens. 5, 6481–6500.

Gao, F., Anderson, M.C., Zhang, X., Yang, Z., Alfieri, J.G., Kustas, W.P., Mueller, R., Johnson, D.M., Prueger, J.H., 2017. Toward mapping crop progress at field scales through fusion of Landsat and MODIS imagery. Remote Sens. Environ. 188, 9–25.

Garrity, D., Becker, M., 1994. Where do green manures fit in Asian rice farming systems, Green Manure Production Systems for Asian Ricelands. In: Selected Papers from the International Rice Research Conference, pp. 1–10.

Griffiths, P., Nendel, C., Hostert, P., 2019. Intra-annual reflectance composites from Sentinel-2 and Landsat for national-scale crop and land cover mapping. Remote Sens. Environ. 220, 135–151.
Gu, Y., Wylie, B.K., Howard, D.M., Phuyal, K.P., Ji, L., 2013. NDVI saturation adjustment: A new approach for improving cropland performance estimates in the Greater Platte River Basin, USA. Ecolog. Indicat. 30, 1–6.
Harris, R.B., 2010. Rangeland degradation on the Qinghai-Tibetan plateau: a review of the evidence of its magnitude and causes. J. Arid Environ. 74, 1–12.
He, G., Zhao, Y., Wang, L., Jiang, S., Zhu, Y., 2019. China's food security challenge: Effects of food habit changes on requirements for arable land and water. J. Cleaner Prod. 229, 739–750.
Hou, X.-Y., Yang, L., Han, Y., 2008. The Significance, Tendency and Suggestions to Grassland Eco-Compensation in China. Chinese J. Grassland 5.
Houborg, R., McCabe, M.F., 2018. Daily Retrieval of NDVI and LAI at 3 m Resolution via the Fusion of CubeSat, Landsat, and MODIS Data. Remote Sens. 10.
Hua, L., Squires, V.R., 2015. Managing China's pastoral lands: Current problems and future prospects. Land Use Policy 43, 129–137.
Huete, A., Didan, K., Miura, T., Rodriguez, E.P., Gao, X., Ferreira, L.G., 2002. Overview of the radiometric and biophysical performance of the MODIS vegetation indices. Remote Sens. Environ. 83, 195–213.
Huilan, W., Yingjun, Q., 2017. Analysis of grassland eco-compensation standard based on the differentiation of the opportunity losses caused by reducing livestock. J. China Agri. University 23.
Jacobs, J., Ward, G., 2012. Effect of intercropping forage peas (Pisum sativum L.) with winter wheat (Tritium vulgare L.) or triticale (Triticale hexaploide Lart.) on DM yield, nutritive characteristics when harvested at different stages of growth. Animal Prod. Sci. 52, 949–958.
Jacobs, J., Ward, G., 2013. Effect of cereal and pea monocultures and combinations and silage additives on whole-crop cereal silage nutritive and fermentation characteristics. Animal production science 53, 427–436.
Jin, Z., Azzari, G., You, C., Di Tommaso, S., Aston, S., Burke, M., Lobell, D.B., 2019. Smallholder maize area and yield mapping at national scales with Google Earth Engine. Remote Sens. Environ. 228, 115–128.
Joshi, N., Baumann, M., Ehammer, A., Fensholt, R., Grogan, K., Hostert, P., Jepsen, M., Kuemmerle, T., Meyfroidt, P., Mitchard, E., Reiche, J., Ryan, C., Waske, B., 2016. A Review of the Application of Optical and Radar Remote Sensing Data Fusion to Land Use Mapping and Monitoring. Remote Sensing 8.
Kearney, J., 2010. Food consumption trends and drivers. Philos. Trans. R Soc. Lond. B Biol. Sci. 365, 2793–2807.
Li, J., Roy, D.P., 2017. A global analysis of Sentinel-2A, Sentinel-2B and Landsat-8 data revisit intervals and implications for terrestrial monitoring. Remote Sens. 9, 902.
Li, X.L., Gao, J., Brierley, G., Qiao, Y.M., Zhang, J., Yang, Y.W., 2013. Rangeland degradation on the Qinghai-Tibet plateau: Implications for rehabilitation. Land Degrad. Dev. 24, 72–80.
Li, Y., Allan Degen, A., Sun, T., Wang, W., Bai, Y., Zhang, T., Long, R., Shang, Z., 2020. Three years of cultivating or fencing lands have different impacts on soil nutrients and properties of a subalpine meadow in the Tibetan plateau. CATENA 186, 104306.
Lithourgidis, A.S., Vasilakoglou, I.B., Dhima, K.V., Dordas, C.A., Yiakoulaki, M.D., 2006. Forage yield and quality of common vetch mixtures with oat and triticale in two seeding ratios. Field Crops Res. 99, 106–113.
Liu, J., Xu, X., Shao, Q., 2008. The spatial and temporal characteristics of grassland degradation in the three-river headwaters region in Qinghai Province. J. Geog. Sci. 18, 259–273.
Liu, J.Y., Kuang, W.H., Zhang, Z.X., Xu, X.L., Qin, Y.W., Ning, J., Zhou, W.C., Zhang, S. W., Li, R.D., Yan, C.Z., Wu, S.X., Shi, X.Z., Jiang, N., Yu, D.S., Pan, X.Z., Chi, W.F., 2014. Spatiotemporal characteristics, patterns, and causes of land-use changes in China since the late 1980s. J. Geog. Sci. 24, 195–210.
Liu, L., Xiao, X., Qin, Y., Wang, J., Xu, X., Hu, Y., Qiao, Z., 2020. Mapping cropping intensity in China using time series Landsat and Sentinel-2 images and Google Earth Engine. Remote Sens. Environ. 239, 111624.
Ma, C., Han, J., 2000. The studies on the optimal time of oat and vetch in both monoculture and mixture in high-cold area. J. Tarim. Univ. Agric. Reclam. 12, 15–19.
Ni, Y., Wang, M., 2019. Spatiotemporal evolution of China's silage corn industry and the factors driving its development. Pratacultural Sci. 36, 1915–1924.
Niu, K., Choler, P., Zhao, B., Du, G., 2009. The allometry of reproductive biomass in response to land use in Tibetan alpine grasslands. Funct. Ecol. 23, 274–283.
Niu, K., Luo, Y., Choler, P., Du, G., 2008. The role of biomass allocation strategy in diversity loss due to fertilization. Basic Appl. Ecol. 9, 485–493.
Olofsson, P., Foody, G.M., Herold, M., Stehman, S.V., Woodcock, C.E., Wulder, M.A., 2014. Good practices for estimating area and assessing accuracy of land change. Remote Sens. Environ. 148, 42–57.
Phiri, D., Morgenroth, J., 2017. Developments in Landsat Land Cover Classification Methods: A Review.
Qin, Z.G., 2004. The current situation of oat research and production, problems and strategy in Tibetan Plateau. 21, 17-21.
Roy, D.P., Kovalskyy, V., Zhang, H., Vermote, E.F., Yan, L., Kumar, S., Egorov, A., 2016. Characterization of Landsat-7 to Landsat-8 reflective wavelength and normalized difference vegetation index continuity. Remote Sens. Environ. 185, 57–70.
Scaramuzza, P., Barsi, J., 2005. Landsat 7 scan line corrector-off gap-filled product development.
Shahrabi, H.S., Ashourloo, D., Rad, A.M., Aghighi, H., Azadbakht, M., Nematollahi, H., 2020. Automatic silage maize detection based on phenological rules using Sentinel-2 time-series dataset. Int. J. Remote Sens. 41, 8406–8427.
Shelestov, A., Lavreniuk, M., Kussul, N., Novikov, A., Skakun, S., 2017. Exploring Google Earth Engine Platform for Big Data Processing: Classification of Multi-Temporal Satellite Imagery for Crop Mapping. Front. Earth Sci. 5.
Shen, M., Zhang, G., Cong, N., Wang, S., Kong, W., Piao, S., 2014. Increasing altitudinal gradient of spring vegetation phenology during the last decade on the Qinghai-Tibetan Plateau. Agric. For. Meteorol. 189–190, 71–80.
Sheng, Y., Song, L., 2019. Agricultural production and food consumption in China: A long-term projection. China Economic Rev. 53, 15–29.
Sidhu, N., Pebesma, E., Camara, G., 2018. Using Google Earth Engine to detect land cover change: Singapore as a use case. European J. Remote Sens. 51, 486–500.
Tang, L., Duan, X., Kong, F., Zhang, F., Zheng, Y., Li, Z., Mei, Y., Zhao, Y., Hu, S., 2018. Influences of climate change on area variation of Qinghai Lake on Qinghai-Tibetan Plateau since 1980s. Sci. Rep. 8, 1–7.
Tilman, D., Clark, M., 2014. Global diets link environmental sustainability and human health. Nature 515, 518-+.
Tucker, C.J., 1979. Red and photographic infrared linear combinations for monitoring vegetation. Remote Sens. Environ. 8, 127–150.
Velho, J.P., Zardin, P.B., Jobim, C.C., Pereira Haygert-Velho, I.M., Moro Alessio, D.R., Giotto, É., Da Conceição, G.M., Gehrke, C.R., 2020. Meta-analysis of corn plants, green fodder (ensilage), and silages of different types of maize hybrids used in experimental conditions in Brazil. Semina Cienc. Agrar. 41, 237–253.
Waldner, F., Chen, Y., Lawes, R., Hochman, Z., 2019. Needle in a haystack: Mapping rare and infrequent crops using satellite imagery and data balancing methods. Remote Sens. Environ. 233, 111375.
Wang, H.C., Liu, D.S., Liu, C.L., Xin-Chun, L.U., Wei, W., Wang, X.X., 2016. Research Progress of Forage Rape and Its Feed Value in China. Soils Crops.
Wang, J., Xiao, X., Liu, L., Wu, X., Qin, Y., Steiner, J.L., Dong, J., 2020a. Mapping sugarcane plantation dynamics in Guangxi, China, by time series Sentinel-1, Sentinel-2 and Landsat images. Remote Sensing of Environment 247.
Wang, J., Xiao, X., Qin, Y., Dong, J., Geissler, G., Zhang, G., Cejda, N., Alikhani, B., Doughty, R.B., 2017. Mapping the dynamics of eastern redcedar encroachment into grasslands during 1984–2010 through PALSAR and time series Landsat images. Remote Sens. Environ. 190, 233–246.
Wang, L., Diao, C., Xian, G., Yin, D., Lu, Y., Zou, S., Erickson, T.A., 2020b. A summary of the special issue on remote sensing of land change science with Google earth engine. Remote Sensing of Environment 248.
Wang, P., Lassoie, J.P., Morreale, S.J., Dong, S., 2015. A critical review of socioeconomic and natural factors in ecological degradation on the Qinghai-Tibetan Plateau, China. Rangeland J. 37, 1–9.
Wardlow, B.D., Egbert, S.L., 2008. Large-area crop mapping using time-series MODIS 250 m NDVI data: An assessment for the U.S. Central Great Plains. Remote Sens. Environ. 112, 1096–1116.
Wen, L., Jinlan, W., Xiaojiao, Z., Shangli, S., Wenxia, C., 2018. Effect of degradation and rebuilding of artificial grasslands on soil respiration and carbon and nitrogen pools on an alpine meadow of the Qinghai-Tibetan Plateau. Ecol. Eng. 111, 134–142.
Wulder, M.A., Loveland, T.R., Roy, D.P., Crawford, C.J., Masek, J.G., Woodcock, C.E., Allen, R.G., Anderson, M.C., Belward, A.S., Cohen, W.B., Dwyer, J., Erb, A., Gao, F., Griffiths, P., Helder, D., Hermosilla, T., Hipple, J.D., Hostert, P., Hughes, M.J., Huntington, J., Johnson, D.M., Kennedy, R., Kilic, A., Li, Z., Lymburner, L., McCorkel, J., Pahlevan, N., Scambos, T.A., Schaaf, C., Schott, J.R., Sheng, Y., Storey, J., Vermote, E., Vogelmann, J., White, J.C., Wynne, R.H., Zhu, Z., 2019. Current status of Landsat program, science, and applications. Remote Sens. Environ. 225, 127–147.
Wulder, M.A., Masek, J.G., Cohen, W.B., Loveland, T.R., Woodcock, C.E., 2012. Opening the archive: How free data has enabled the science and monitoring promise of Landsat. Remote Sens. Environ. 122, 2–10.
Xiao, X., Boles, S., Frolking, S., Li, C., Babu, J.Y., Salas, W., III, B.M., 2005a. Mapping paddy rice agriculture in South and Southeast Asia using multi-temporal MODIS images. Remote Sensing of Environment 100, 95-113.
Xiao, X., Boles, S., Frolking, S., Li, C., Babu, J.Y., Salas, W., III, B.M., 2006. Mapping paddy rice agriculture in South and Southeast Asia using multi-temporal MODIS images. Remote Sensing of Environment 100, 95-113.
Xiao, X., Boles, S., Liu, J., Zhuang, D., Frolking, S., Li, C., Salas, W., III, B.M., 2005b. Mapping paddy rice agriculture in southern China using multi-temporal MODIS images. Remote Sensing of Environment 95, 480-492.
Xue, B., Zhao, X.Q., Zhang, Y.S., 2005. Seasonal changes in weight and body composition of yak grazing on alpine-meadow grassland in the Qinghai-Tibetan plateau of China1. J. Anim. Sci. 83, 1908–1913.
Yang, D., Hao, L., Liu, S., Niu, J., 2018. The research progress of nutritive value of ruminant animal's common forage in Qinghai Province. Feed Industry 01.
Yang, J.L., Dong, J.W., Xiao, X.M., Dai, J.H., Wu, C.Y., Xia, J.Y., Zhao, G.S., Zhao, M.M., Li, Z.L., Zhang, Y., Ge, Q.S., 2019. Divergent shifts in peak photosynthesis timing of temperate and alpine grasslands in China. Remote Sens. Environ. 233, 14.
Zhai, S., Chen, Q., Wang, W., 2019. What drives green fodder supply in China?-A Nerlovian analysis with LASSO variable selection. Sustainability (Switzerland) 11.
Zhang, G., Xiao, X., Dong, J., Kou, W., Jin, C., Qin, Y., Zhou, Y., Wang, J., Menarguez, M. A., Biradar, C., 2015a. Mapping paddy rice planting areas through time series analysis of MODIS land surface temperature and vegetation index data. ISPRS J. Photogramm. Remote Sens. 106, 157–171.
Zhang, G., Zhang, Y., Dong, J., Xiao, X., 2013a. In: Proceedings of the National Academy of Sciences of the United States of America, pp. 4309–4314.
Zhang, L., Fan, J., Zhou, D., Zhang, H., 2017. Ecological protection and restoration program reduced grazing pressure in the Three-River Headwaters Region, China. Rangeland Ecol. Manage. 70, 540–548.

Zhang, R., Wang, S.a., Gao, W., Sun, W., Wang, J., Niu, L., 2015b. Remote-sensing classification method of county-level agricultural crops using time-series NDVI. Transactions of the Chinese Society for Agricultural Machinery 46, 246-252.

Zhang, W., Li, A., Jin, H., Bian, J., Zhang, Z., Lei, G., Qin, Z., Huang, C., 2013b. An Enhanced Spatial and Temporal Data Fusion Model for Fusing Landsat and MODIS Surface Reflectance to Generate High Temporal Landsat-Like Data. Remote Sensing 5, 5346–5368.

Zhang, Y., Zhou, X., Wang, Q., 1998. A Preliminary Analysis of Production Performance of Oat (Avena sativa) at Alpine Meadow Pasture. Acta Agrestia Sinica.

Zhang, Z., Duan, J., Wang, S., Luo, C., Chang, X., Zhu, X., Xu, B., Wang, W., 2012. Effects of land use and management on ecosystem respiration in alpine meadow on the Tibetan plateau. Soil Tillage Res. 124, 161–169.

Zhao, J., Zhong, Y., Hu, X., Wei, L., Zhang, L., 2020. A robust spectral-spatial approach to identifying heterogeneous crops using remote sensing imagery with high spectral and spatial resolutions. Remote Sens. Environ. 239, 111605.

Zhong, L., Gong, P., Biging, G.S., 2014. Efficient corn and soybean mapping with temporal extendability: A multi-year experiment using Landsat imagery. Remote Sens. Environ. 140, 1–13.

Zhong, Y., Wang, X., Xu, Y., Wang, S., Jia, T., Hu, X., Zhao, J., Wei, L., Zhang, L., 2018. Mini-UAV-Borne Hyperspectral Remote Sensing: From Observation and Processing to Applications. IEEE Geosci. Remote Sens. Mag. 6, 46–62.

Zhou, Y., Dong, J., Liu, J., Metternicht, G., Shen, W., You, N., Zhao, G., Xiao, X., 2019. Are There Sufficient Landsat Observations for Retrospective and Continuous Monitoring of Land Cover Changes in China? Remote Sensing 11, 1808.

Zhou, Y., Xiao, X., Qin, Y., Dong, J., Zhang, G., Kou, W., Jin, C., Wang, J., Li, X., 2016. Mapping paddy rice planting area in rice-wetland coexistent areas through analysis of Landsat 8 OLI and MODIS images. Int. J. Appl. Earth Obs. Geoinf. 46, 1–12.

Zhu, Z., Wang, S., Woodcock, C.E., 2015. Improvement and expansion of the Fmask algorithm: Cloud, cloud shadow, and snow detection for Landsats 4–7, 8, and Sentinel 2 images. Remote Sens. Environ. 159, 269–277.

Zhu, Z., Woodcock, C.E., 2012. Object-based cloud and cloud shadow detection in Landsat imagery. 118, 0-94.